Supplementary Information

Interfacial stress induced by the adaptive construction of hydrangea-like heterojunctions based on in situ electrochemical phase reconfiguration for highly efficiency oxygen evolution reaction at high current density

Yanling Qiu [a], Aowei Sun [a], Xinyue Zhang [a], Xiuping Liu [b], Yijun Wang [b,c,]*, and Jingquan Liu [a,b,]*

[a] College of Materials Science and Engineering, Institute for Graphene Applied Technology Innovation, Qingdao University, Qingdao 266071, China

[b] College of Materials Science and Engineering, Linyi University, Linyi, 276000 Shandong, China.

[c] Philippine Christian University Center for International Education, Philippine Christian University, Manila, 1004 Metro Manila, Philippine

*Corresponding Author. E-Mail: wangyijun@lyu.edu.cn; jliu@qdu.edu.cn

1 Experimental section

1.1 Materials

The nickel foam (NF) was purchased from Kunshan Resker Electronic Technology Co., Ltd. Absolute ethyl alcohol and hydrochloric acid (HCl, 12 M) were purchased from Shanghai Zhentai Chemical Co., Ltd. Potassium hydroxide (KOH), selenium powder (Se, 99.9%) and sodium borohydride ($NaBH_4$, 98%) were purchased from Shandong Kepler Biotechnology Co., Ltd. All chemical regents were used as received without further purification. Deionized (DI) water was made by the Millipore system with a resistivity of 18 $M\Omega \cdot cm^{-1}$ and used in all experiments.

1.2 Materials synthesis

1.2.1 Synthesis of NiSe nanorod arrays on NF

In a typical synthesis, NF (2×3 cm^2) was firstly treated with 5% HCl for 10 minutes, then rinsed with plenty of DI water and ethanol. 0.15792 g Se powder and 0.15132 g $NaBH_4$ were dissolved in 2 mL aqueous solution, then diluted to 40 mL and stirred until fully dissolved. A 50 mL Teflon-lined autoclave was treated with aqua regia for 12 h. Here is to create an environment in which NO_3^- exists for the next hydrothermal coordination reaction. Then, the above completely dissolved solution was transferred into a 50 mL Teflon-lined autoclave, and NF was placed in the autoclave slantways. The autoclave was kept at 160 °C for 24 h. After the reaction, a united dark gray Ni_xSe_y sample was formed on NF substrate, which was thoroughly rinsed with DI water and ethanol, and then dried in the oven at 60 °C overnight.

1.2.2 Preparation of RuO$_2$ electrodes

5 mg of RuO_2 was mixed with 450 μL of deionized water, 450 μL of absolute ethanol, and 20 μL of Nafion (5 wt%), and the resulting mixture was sonicated for 60 min to obtain RuO_2 ink. Then use a pipette to draw 2 μL ink each time, which was carefully dropped onto the NF and then dried naturally at room temperature. The total ink added was 38 μL, which was dropped in 19 times for the coating. Using this method, RuO_2 electrodes were prepared separately. The loading of RuO_2 on NF is 0.82 mg cm^{-2}.

1.3 Materials characterizations

The morphological characterizations of the samples were performed by SEM (Hitachi S-4800) with 30 kV accelerating voltage and TEM, HRTEM (Zeiss Libra 200 FE) operated at 200 kV. The energy-dispersive X-ray (EDX) elemental mapping was collected on an SEM with 60 kV accelerating voltage. The crystal structures of the samples were studied by XRD (Rigaku D-MAX-RB 12 KW). The surface elemental composition and chemical valence states of substances were investigated by XPS (Thermo Scientific K-Alpha). The chemical bond compositions of the samples were analyzed by FT-IR spectrometer (Bruker spectrometer, Tensor 27). Inductively coupled plasma optical emission spectroscopy (ICP-AES) analysis was conducted on a Thermo ICAP PRO spectrometer. Electron paramagnetic resonance (EPR) spectra in the X-band were obtained on a Bruker EMX PLUS spectrometer and calibrated with a DPPH standard (g = 2.0036). Raman spectroscopy was carried out by using a Horiba Raman spectrometer equipped with an Olympus BX41 microscope and a Spectra-Physics 532-nm Ar laser.

All electrochemical measurements were carried out on the electrochemical

workstation (CHI 760 E, Shanghai Chenhua Instrument Corporation, China) in 1 M KOH (pH = 13.8). The electrocatalytic performance of the samples was investigated in a typical three-electrode system with the samples as working electrodes, the Hg/HgO electrode and platinum foil as the reference and counter electrode, respectively. The electrode size is around 1.0×0.5 cm^2, and the effective area immersed in the electrolyte is (0.5×0.5 cm^2) for various samples. The equation for IR correction of LSV curve: E vs. RHE = E vs. Hg/HgO + (0.098 + 0.0591 pH) V, and overpotential for OER was η = E vs. RHE – 1.23 V. The OER polarization curves were tested using the linear sweep voltammetry (LSV) technique at a scan rate of mV·s^{-1}. Cyclic voltammetry (CV) was employed to estimate the double-layer capacitance (Cdl) in a non-Faradaic potential range. In order to perform a more comprehensive test of the material, the Electrochemical impedance spectroscopy (EIS)

 test of the electrode material was carried out under the operating conditions of OER. A test voltage is applied to the material and the test was performed in a scanning frequency range from 100 kHz to 10 MHz. To evaluate the long-term durability of NF-LDF-O, the sample was subject to chronopotentiometry (C-P) testing at 50 and 500 mA cm^{-2} for 100 h. All of the tests were carried out at room temperature, and the current densities were normalized concerning the geometric area of the working electrodes.
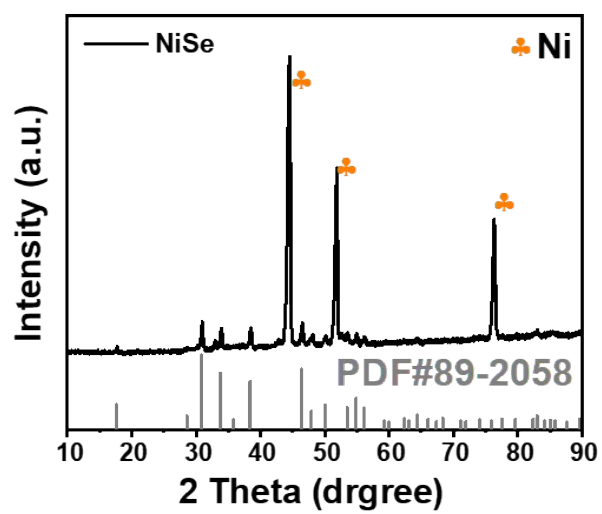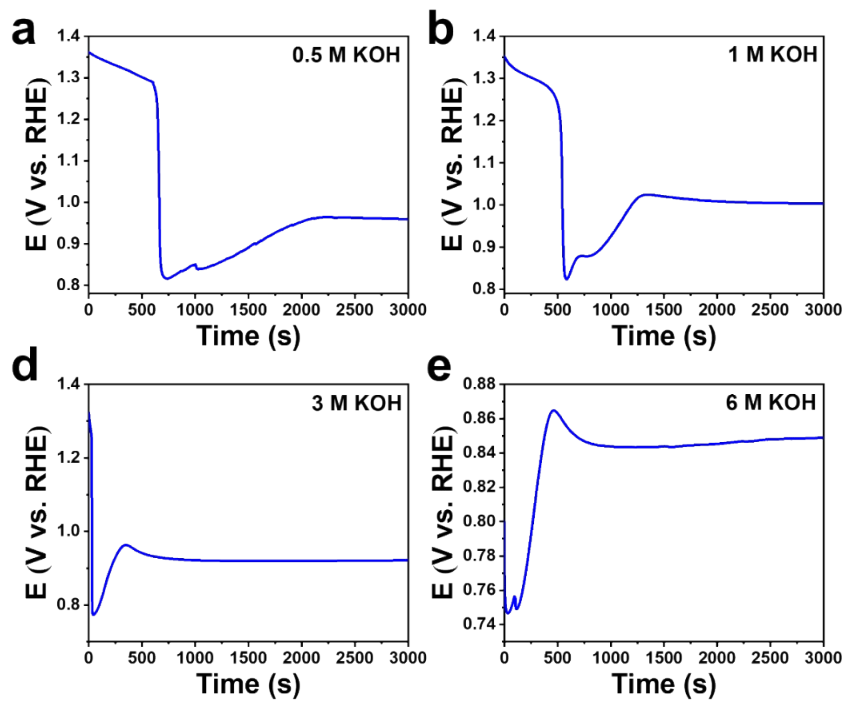
Fig. S1 The XRD pattern of NS.
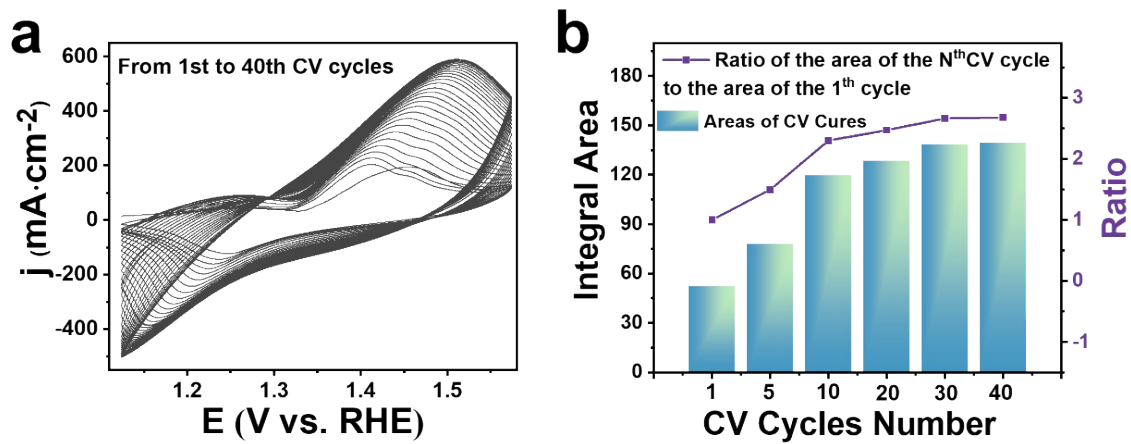
Fig. S2 (a) The Operando CV curves for the NS electrode from 1 to 40 cycles at the scan rate of 5 mV s^{-1}. (b) The integral areas of the CV curves of the NS electrode in different CV cycles and the ratio of its area to the CV area of the first cycle.
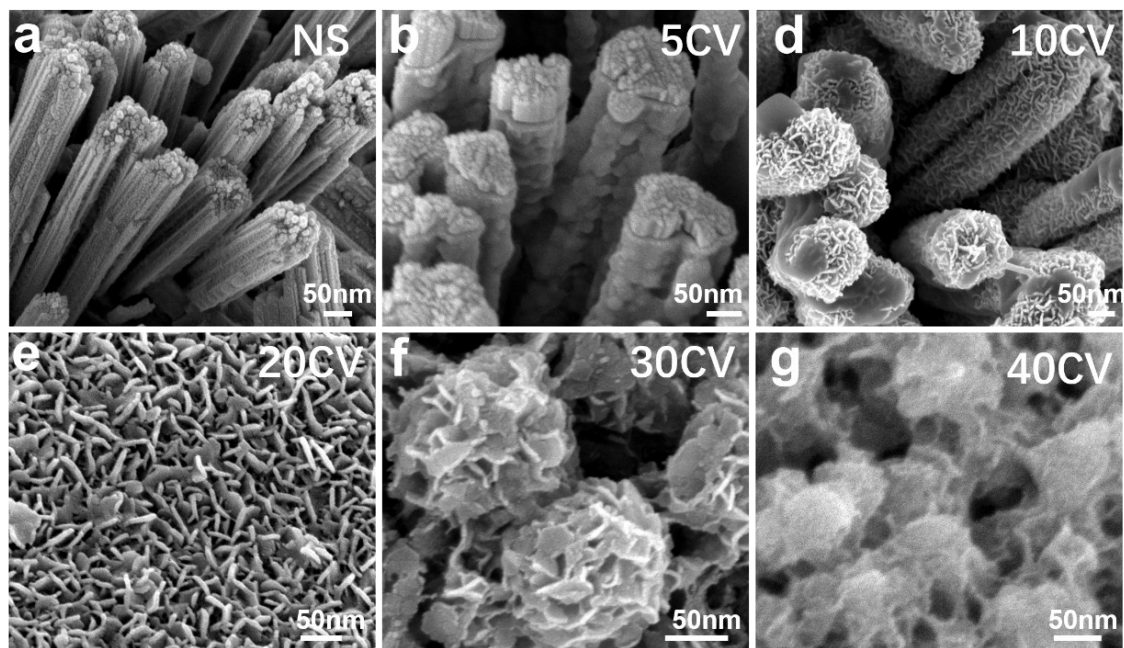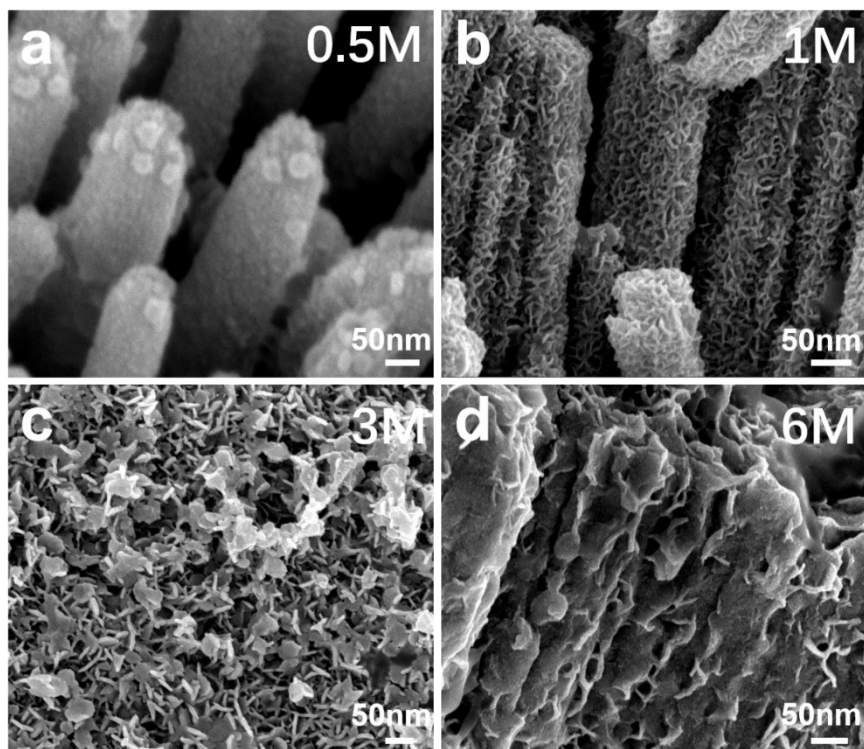
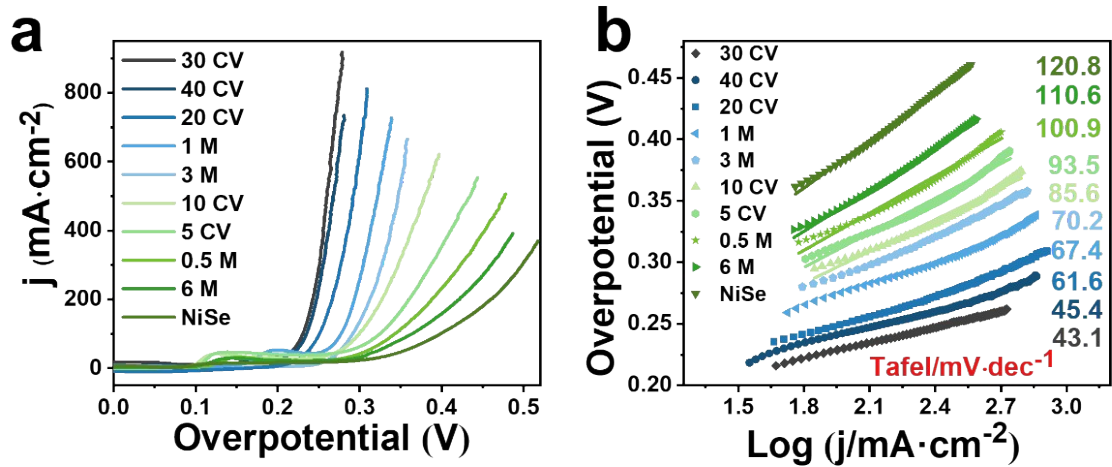**Fig. S3** The SEM images of NS after different cycles.

Fig. S4 The galvanostatic CP curves of NS catalyst at low current densities in (a) 0.5 M, (b) 1 M, (c) 3 M and (d) 6 M KOH electrolyte solutions.
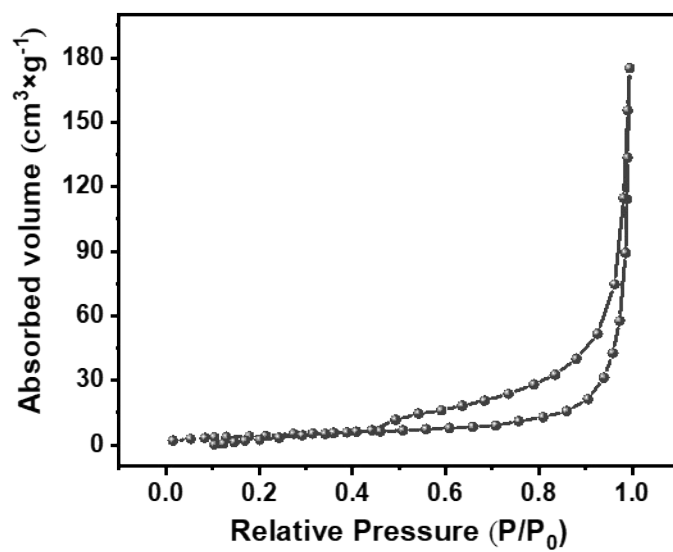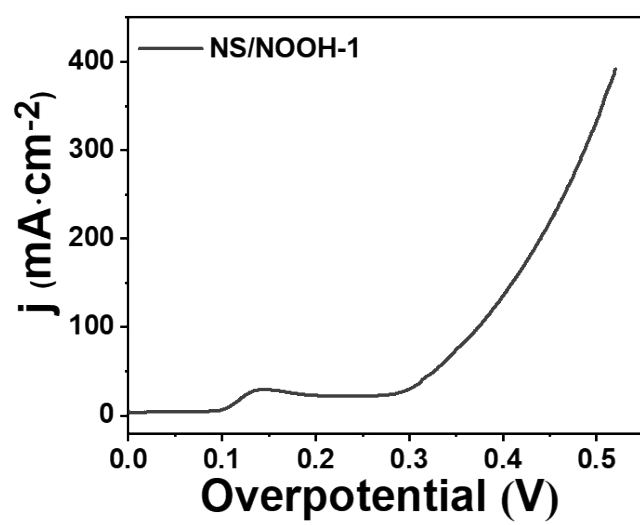
Fig. S5 (a) The SEM images of NS catalyst after CP tests at low current densities in (a) 0.5 M, (b) 1 M, (c) 3 M and (d) 6 M KOH electrolyte solutions.
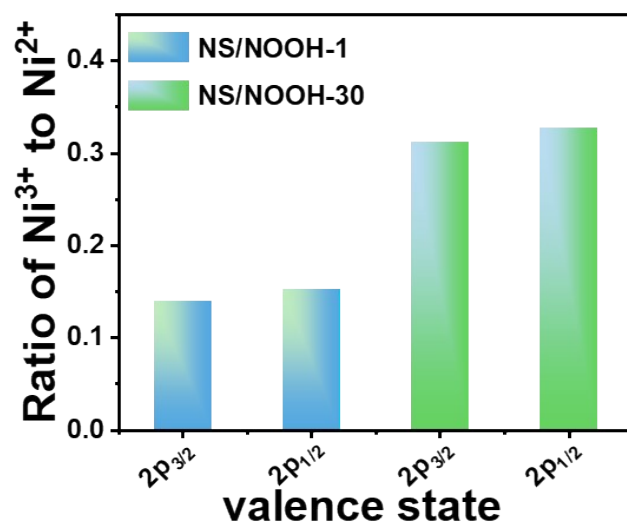
Fig. S6 (a) LSV curves and (b) Tafel plots of NS after different CV cycles and CP tests at low current densities in KOH electrolyte solutions with different concentrations.
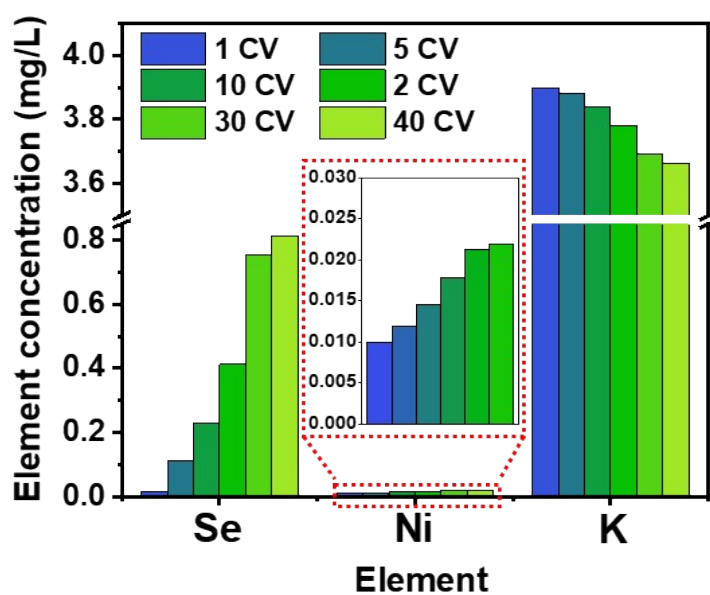
Fig. S7. The nitrogen absorption-desorption isotherm of the NS/NOOH-30.

Fig. S8 The LSV curves of NS after 1 CV cycle.

Fig. S9 The molar ratio of Ni^{3+}/Ni^{2+} on the surface of NS/NOOH-1 and NS/NOOH-30 electrode.

Fig. S10 The contents of Se, Ni and K ions in the withdrawn solution after different CV cycles of the samples. The inset is an enlarged view of a bar chart of the contents of Ni ions. The above contents of Se, Ni and K ions were obtained by diluting the test extraction solution 10 times, 1 time and 20 times, respectively.
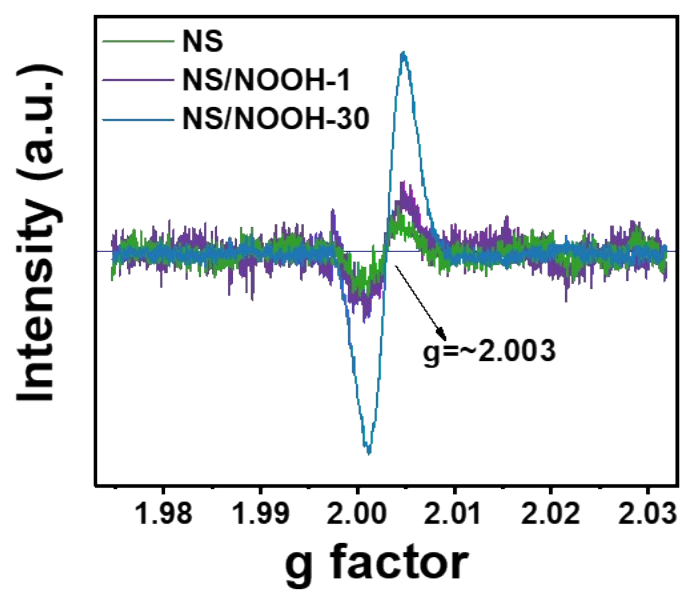
Fig. S11 The EPR spectra of NS, NS/NOOH-1 and NS/NOOH-30.
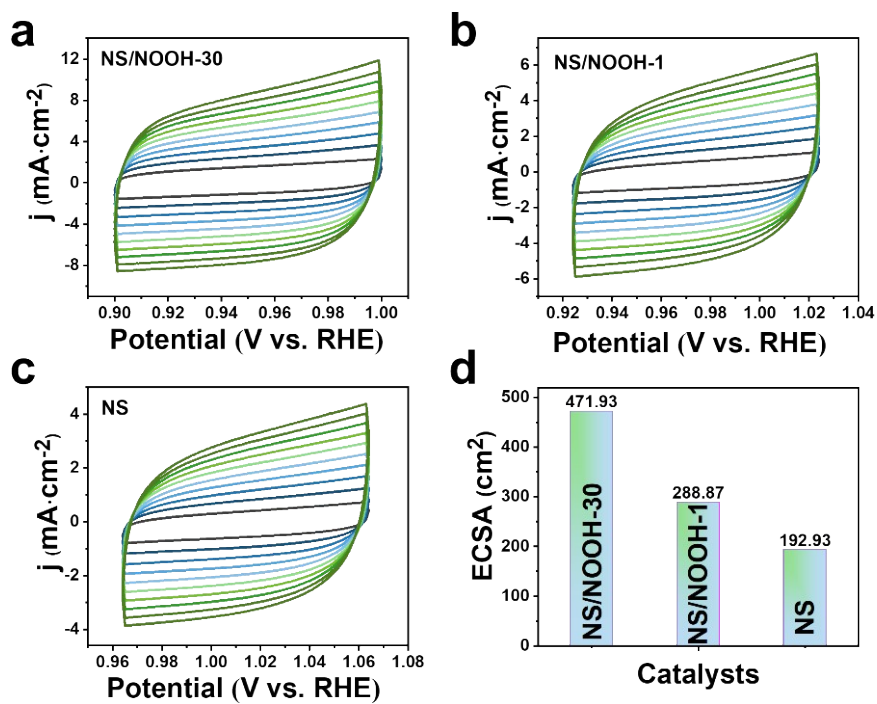
Fig. S12 The CV curves with the scan rate of 10-100 mV/s for (a) NS/NOOH-30, (b) NS/NOOH-1 and (c) NS. (d) ECSA values calculated from Cdl.

Fig. S13. The LSV curves normalized by ECSA of NS, NS/NOOH-1 and NS/NOOH-30.

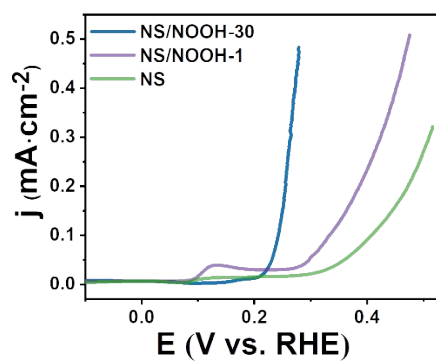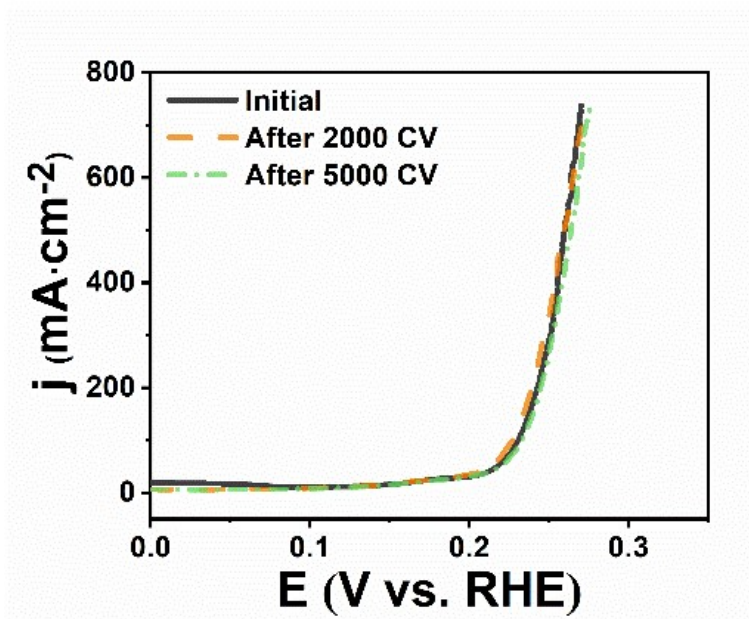**Fig. S14** The LSV curves of NS/NOOH-30 before and after exposure to 2000 and 5000

CVs.

Table S1 The overpotentials at the current densities of 50 and 500 mA·cm^{-2} and Tafel slope of different samples.

Catalyst NS/NOOH-	η_{50} (mV)	η_{500} (mV)	Tafel slope (mV·dec^{-1})
0 CV	353	--	120.8
5 CV	284	434	93.5
10 CV	274.5	379	85.6
20 CV	237.2	291.8	61.6
30 CV	220	260	43.1
40 CV	221.2	267.5	45.4
0.5 M	308	476.5	100.9
1M	256	321.8	67.4
3 M	275.4	346.5	70.2
6 M	321	--	110.6

Table S2 Comparison of OER performances of NS/NOOH-30 with those of other electrocatalysts recently reported in 1.0 M KOH.

Catalyst	j(mA·cm^{-2})	potential (mV)	Ref.
NS/NOOH-30	50	207	This work
	500	266	
NiSe@NiOOH/NF	50	332	[1]
2D Fe-doped NiSe NSs	10	282.7	[2]
FeOOH@Fe-NiSe@NiFe	10	224	[3]
CoSe-0.2/NiSe-nrs/NF	100	310	[4]
NiOOH/FeOOH NBs	10	228	[5]
V-Ni3S2@NiOOH	20	248	[6]
Fe-doped NiOOH	10	210	[7]
NiFe$_2$O$_{4-x}$Se$_x$/NiOOH	10	153	[8]
	500	259	
Mo-NiOOH nanosheets	100	390	[9]
Fe-NiOOH@CC	20	351	[10]
NiSe/Ni/NC	10	312	[11]
Pt-Ni$_3$Se$_2$@NiOOH/NF	50	310	[12]

NiFeCo-S/C	10	271	13
(FeNi)O/NiSe@NF	20	268	14
NiSe@CoFe LDH/NF	10	203	15
	100	236	
FeNiOxHy/NF	10	195	16
	1000	306	
$Ni_xCo_{1-x}OOH$	10	350	17
AlOOH NFs adsorbed with Fe^{III}/Ni^{II}	10	275	18
(Ni, Fe)Se@NiFe-LDH/NF	100	253	19
MoS_2@NiOOH@C-MC	10	280	20
NiSe@NiFe-LDH heterojunction	500	302	21
$Cu-NiP_x/NiSe_y$	100	264	22
$(Zn-Fe_xNi_{(1-x)})OOH$	1000	330	23
$N-MoS_2 \cdot Ni_3S_2/NiS$	10	231	24
NiOOH@FeOOH	500	292	25

References

1. X. Li, G. Q. Han, Y. R. Liu, B. Dong, W.-H. Hu, X. Shang, Y. M. Chai and C. G. Liu, *ACS Appl. Mater. Inter.*, 2016, **8**, 20057-20066.

2. K. Chang, D. T. Tran, J. Wang, N. H. Kim and J. H. Lee, *J. Mater. Chem. A*, 2022, **10**, 3102-3111.

3. P. Wang, Y. Lin, Q. Xu, L. Wan, Z. Xu and B. Wang, *Ind. Eng. Chem. Res.*, 2021, DOI: 10.1021/acs.iecr.1c02592.

4. J. Du, S. You, X. Li, B. Tang, B. Jiang, Y. Yu, Z. Cai, N. Ren and J. Zou, *ACS Appl. Mater. Inter.*, 2020, **12**, 686-697.

5. P. Yan, Q. Liu, H. Zhang, L. Qiu, H. B. Wu and X.-Y. Yu, *J. Mater. Chem. A*, 2021, **9**, 15586-15594.

6. Y. Wang, J. Liu, Y. Liao, C. Wu and Y. Chen, *J. Alloy. Compd.*, 2021, **856**, 158219.

7. B. Kim, M. K. Kabiraz, J. Lee, C. Choi, H. Baik, Y. Jung, H. S. Oh, S. I. Choi and K. Lee, *Matter*, 2021, **4**, 3585-3604.

8. Y. Huang, J. J. Wang, Y. Zou, L. W. Jiang, X. L. Liu, W. J. Jiang, H. Liu and J. S. Hu, *Chinese J. Catal.*, 2021, **42**, 1395-1403.

9. Y. Jin, S. Huang, X. Yue, C. Shu and P. K. Shen, *Int. J. Hydrogen Energ.*, 2018, **43**, 12140-12145.

10. L. Yi, Y. Niu, B. Feng, M. Zhao and W. Hu, *J. Mater. Chem. A*, 2021, **9**, 4213-4220.

11. J. Ding, P. Wang, S. Ji, H. Wang, D. J. L. Brett and R. Wang, *Electrochimica Acta*, 2019, **300**, 93-101.

12. X. Zheng, Y. Cao, X. Han, H. Liu, J. Wang, Z. Zhang, X. Wu, C. Zhong, W. Hu and Y. Deng, *Sci. China Mater.*, 2019, **62**, 1096-1104.

13. M. H. Han, M. W. Pin, J. H. Koh, J. H. Park, J. Kim, B. K. Min, W. H. Lee and H.-S. Oh, *J. Mater. Chem. A*, 2021, **9**, 27034-27040.

14. W. Dai, Y. a. Zhu, Y. Ye, Y. Pan, T. Lu and S. Huang, *J. Colloid Inter. Sci.*, 2022, **608**, 3030-3039.

15. F. Nie, Z. Li, X. Dai, X. Yin, Y. Gan, Z. Yang, B. Wu, Z. Ren, Y. Cao and W. Song, *Chem. Eng. J.*, 2022, **431**, 134080.

16. H. S. Hu, S. Si, R. J. Liu, C. B. Wang and Y. Y. Feng, *Int. J. Energ. Res.,* 2020, **44**, 9222-9232.

17. L. A. Huang, Z. He, J. Guo, S. E. Pei, H. Shao and J. Wang, *Nano Res.*, 2020, **13**, 246-254.

18. Y. Zhou and H. C. Zeng, *ACS Sustain. Chem. Eng.*, 2019, **7**, 5953-5962.

19. J. Hu, Y. Q. Liang, S. L. Wu, Z. Y. Li, C. S. Shi, S. Y. Luo, H. J. Sun, S. L. Zhu and Z. D. Cui, *Mater. Today Nano*, 2022, **17**, 100150.

20. J. Liu, S. Zhao, C. Wang, Y. Ma, L. He, B. Liu and Z. Zhang, *J. Colloid Inter. Sci.*, 2022, **608**, 1627-1637.

21. W. Bao, C. Yang, T. Ai, J. Zhang, L. Zhou, Y. li, X. Wei, X. Zou and Y. Wang, *Fuel*, 2023, **332**, 126227.

22. B. Han, X. Du, J. Li, H. Wang, G. Liu and J. Li, *Appl. Surf. Sci.*, 2022, **604**, 154617.

23. X. Zhang, H. Yi, M. Jin, Q. Lian, Y. Huang, Z. Ai, R. Huang, Z. Zuo, C. Tang, A.

Amini, F. Jia, S. Song and C. Cheng, *Small*, 2022, **18**, 2203710.

24. Y. Gao, J. Li, H. Gong, C. Zhang, H. Fan, X. Xie, X. Huang, H. Xue, T. Wang and J. He, *J. Mater. Chem. A*, 2022, **10**, 11755-11765.

25. B. Wu, S. Gong, Y. Lin, T. Li, A. Chen, M. Zhao, Q. Zhang and L. Chen, *Adv. Mater.*, 2022, 2108619.